Angiography-based superficial wall strain of de novo stenotic coronary arteries

Wu, Xinlei; Renkens, Mick P.L.; Kerkmeijer, Laura; Lunardi, Mattia; Huang, Jiayue; Ding, Daixin; O'Leary, Neil; de Winter, Robbert J.; Onuma, Yoshinobu; Serruys, Patrick W.

Published in:
Cardiovascular Revascularization Medicine

DOI:
10.1016/j.carrev.2023.03.005

Cardiovascular Revascularization Medicine 53 (2023) 51–60

Contents lists available at ScienceDirect

Cardiovascular Revascularization Medicine

Angiography-Based Superficial Wall Strain of De Novo Stenotic Coronary Arteries: Serial Assessment of Vessels Treated with Bioresorbable Scaffold or Drug-Eluting Stent☆

Xinlei Wu [a,1], Mick P.L. Renkens [b], Laura Kerkmeijer [c], Mattia Lunardi [a], Jiayue Huang [a], Daixin Ding [a], Neil O'Leary [a], Robbert J. de Winter [b], Yoshinobu Onuma [a], Patrick W. Serruys [a], Joanna Wykrzykowska [b,d], Shengxian Tu [e], William Wijns [a,*]

[a] The Lambe Institute for Translational Medicine, Smart Sensors Laboratory, Corrib Core Laboratory and Curam, University of Galway, Ireland
[b] Amsterdam UMC, Heart Center, University of Amsterdam, Amsterdam, the Netherlands
[c] Isala Heart Center, Zwolle, the Netherlands
[d] UMC Groningen, Thorax Center, University of Groningen, Groningen, the Netherlands
[e] Med-X Research Institute, Shanghai Jiao Tong University, China

ARTICLE INFO

Article history:
Received 14 March 2023
Accepted 14 March 2023
Available online 22 March 2023

Keywords:
Superficial wall strain
Quantitative coronary angiography
Bioresorbable scaffold
Drug-eluting stent

ABSTRACT

Objectives: This study sought to present an angiography-based computational model for serial assessment of superficial wall strain (SWS, dimensionless) of de-novo coronary stenoses treated with either bioresorbable scaffold (BRS) or drug-eluting stent (DES).
Background: A novel method for SWS allows the assessment of the mechanical status of arteries in-vivo, which may help for predicting cardiovascular outcomes.
Methods: Patients with arterial stenosis treated with BRS ($n = 21$) or DES ($n = 21$) were included from ABSORB Cohort B1 and AIDA trials. The SWS analyses were performed along with quantitative coronary angiography (QCA) at pre-PCI, post-PCI, and 5-year follow-up. Measurements of QCA and SWS parameters were quantified at the treated segment and adjacent 5-mm proximal and distal edges.
Results: Before PCI, the peak SWS on the 'to be treated' segment (0.79 ± 0.36) was significantly higher than at both virtual edges (0.44 ± 0.14 and 0.45 ± 0.21; both $p < 0.001$). The peak SWS in the treated segment significantly decreased by 0.44 ± 0.13 ($p < 0.001$). The surface area of high SWS decreased from 69.97mm^2 to 40.08mm^2 ($p = 0.002$). The peak SWS in BRS group decreased to a similar extent ($p = 0.775$) from 0.81 ± 0.36 to 0.41 ± 0.14 ($p < 0.001$), compared with DES group from 0.77 ± 0.39 to 0.47 ± 0.13 ($p = 0.001$). Relocation of high SWS to device edges was often observed in both groups after PCI (35 of 82 cases, 41.7 %). At follow-up of BRS, the peak SWS remained unchanged compared to post-PCI (0.40 ± 0.12 versus 0.36 ± 0.09, $p = 0.319$).
Conclusion: Angiography-based SWS provided valuable information about the mechanical status of coronary arteries. Device implantation led to a significant decrease of SWS to a similar extent with either polymer-based scaffolds or permanent metallic stents.

1. Introduction

In vivo quantification of the mechanical status of coronary plaque may be helpful for the diagnosis, prognosis and evaluation of treatment strategies in acute and chronic coronary syndromes [1]. Abnormal mechanical status of diseased coronary arterial segments could elicit tears of the superficial wall with cracks propagating to the underlying necrotic core, eventually leading to acute plaque events and occlusive thrombosis [2,3].

A new and validated angiography-based technique, called 4-dimensional superficial wall strain (4D-SWS) [2,4,5], enables the

Abbreviations: AS%, percent area stenosis; BRS, bioresorbable scaffold; D, dimensional; DES, drug-eluting stent; DS%, percent diameter stenosis; MLA, minimum lumen area; MLD, minimum lumen diameter; PCI, percutaneous coronary intervention; QCA, quantitative coronary angiography; SWS, superficial wall strain.

☆ This work was supported by Science Foundation Ireland (15/RP/2765) and by the Natural Science Foundation of Zhejiang Province, China (LQ20H180004).

* Corresponding author at: SFI Research Professor in Interventional Cardiology, University of Galway (UoG), Ireland University Road, Galway H91 TK33, Ireland.
E-mail address: William.Wyns@universityofgalway.ie (W. Wijns).
[1] Current address of Xinlei Wu: Institute of Cardiovascular Development and Translational Medicine, the Second Affiliated Hospital of Wenzhou Medical University, Wenzhou, China

https://doi.org/10.1016/j.carrev.2023.03.005

evaluation of the mechanical status of coronary arterial wall by extracting the time-varying morphology of lumen-wall interface in vivo [4,5]. The local deformation data of the superficial wall during the cardiac cycle are obtained by measurement of the dynamic displacement of finite element (a numerical computation technique) from angiography [6]. Because the deformations of superficial wall are calculated in 3D space, SWS values (dimensionless) represent the combination of three deformation components of cylindrical coordinates (i.e. circumferential, longitudinal, and radial directions). Previous work has indeed reported that sites of late plaque rupture as confirmed by angiography and optical coherence tomography during acute coronary syndromes often co-localized with high SWS at baseline [2].

Percutaneous coronary intervention (PCI) can influence the compositional structure of plaque and physiological function of stenotic arteries by altering their morphological and mechanical status [7–9]. Conversely, cyclic variations of the mechanical status of the superficial wall may interfere with the performance of metallic stents or scaffolds through device fatigue and fracture [10], as well as nonuniform absorption in the case of biodegradable implants, all of which can potentially lead to device-related complications [11].

Thus, the purposes of the present study were 1) to comprehensively assess the SWS of de novo stenotic arteries in vivo; 2) to quantitate acute changes in SWS post-PCI between implantation of two different device platforms (drug-eluting stent [DES] vs. bioresorbable scaffold [BRS]); 3) to compare serial changes in SWS after BRS implant and its full resorption at 5-year follow-up.

2. Methods

2.1. Study design and population

This was an observational mechanistic study of angiography-based SWS. We selected angiograms from a subset of patients enrolled in the ABSORB Cohort B trial (NCT00856856) [12] or the AIDA trial (NCT01858077) [13]. The ethics committee at each participating institution approved the corresponding protocol and patients gave written informed consent before inclusion. Angiographic data in patients who underwent successful PCI were selected for this post-hoc analysis based on the following inclusion criteria: 1) At least one native major epicardial coronary arteries with de novo lesions was treated with BRS or DES; 2) Angiographic imaging with two projections ≥25° apart was obtained by flat-panel systems; 3) Complete contrast filling of the interrogated vessel. Exclusion criteria were: 1) Excessive overlap or foreshortening (>90 %); 2) Insufficient angiographic image quality preventing delineation of lumen contours; 3) Contrast filling not consistently achieved over at least one entire cardiac cycle; 4) There is only one projection view of the stenotic artery; 5) Prior coronary artery bypass graft. All patients ($n = 14$) in the subgroup of ABSORB Cohort B trial were treated with a BRS device 3.0 mm in diameter and 18 mm in length. Eligible patients enrolled in the AIDA trial who received the same size (3 mm × 18 mm) BRS or DES were included for this analysis ($n = 24$).

2.2. Treatment procedure and devices

Target lesions were treated using standard interventional techniques that included mandatory pre-dilation with a balloon shorter and 0.5-mm smaller in diameter than the implanted device. The BRS was implanted at a pressure not exceeding the rated burst pressure (16 atm). Post-dilation with a balloon shorter than the implanted device was recommended at the discretion of the operator, as was bailout treatment.

The BRS (Abbott Vascular, Santa Clara, CA, USA) is a device consisting of a backbone of a fully resorbable polymer (poly-L-lactide), coated with a copolymer (poly-D-L-lactide, PLLA) that contains and releases the anti-proliferative drug (everolimus) with a strut thickness of 157 μm [14]. Two platinum markers at each end outline the boundaries of the scaffold and allow scaffold edges visualization on angiography. The XIENCE V stent (Abbott Vascular) is a metallic platform composed of medical grade L-605 cobalt-chromium alloy with a strut thickness of ~90 μm, coated with a biocompatible fluorinated copolymer that contains and releases the antiproliferative drug (everolimus). Of note, the mechanical strength of polymer-based scaffolds (tensile modulus: 3.1–3.7 GPa) is much weaker than that of the metallic-based DES platforms (tensile modulus: 210–235 GPa) [14].

2.3. Quantitative coronary angiography analysis

Angiographic images were recorded by monoplane or biplane X-ray systems (AXIOM-Artis, Siemens, Malvern, Pennsylvania; AlluraXper, Philips Healthcare, Best, the Netherlands; INTEGRIS Allura, Philips Healthcare; Innova 3100, GE Healthcare, Chalfont, Buckinghamshire, United Kingdom). The 3D angiographic reconstruction at consecutive timepoints within one cardiac cycle was performed by an experienced analyst (X.W.) using a validated software (QAngio XA 3D, Medis BV, Leiden, the Netherlands). The synchronization between two projections was performed from the electrocardiogram or according to the different stages of vessel motion during heart contraction and relaxation [6]. The proximal and distal ends of the interrogated arteries were selected from anatomic landmarks such as bifurcations. The following quantitative coronary angiography (QCA) parameters were analyzed: minimum lumen diameter (MLD), minimum lumen area (MLA), percent diameter stenosis (DS%), and percent area stenosis (AS%). The acute gain in MLD was calculated as MLD change between before and after PCI.

2.4. Superficial wall strain analysis

Details of the SWS analysis have been previously described [5,6]. Briefly, for each vessel, all reconstructed geometries within one cardiac cycle were discretized into structured grids with the identical node numbers in longitudinal and circumference. The predicted cyclic motion of the arteries was determined based on the principle of minimum potential energy, when all nodes between two consecutive configurations are matched to generate the one-to-one mapping relationship. The initial configuration for cyclic computation was selected at diastasis (i.e., mid-diastole), because the heart is quiescent at this cardiac phase when the kinetic and strain energy of the coronary arteries are at the lowest level throughout the entire cardiac cycle [2,4,5]. Starting from diastasis, the SWS can be calculated by dividing the finite element length of structured grids at the next timepoint by that at the previous one by using a validated algorithm [5].

To quantitatively assess the mechanical status of the coronary superficial layer, three parameters were obtained from the SWS analysis, including peak SWS, segment-averaged SWS and time-averaged SWS (see Table 1 for definitions). Another derivative spatial quantity, the surface area of high SWS, was calculated to highlight the region with SWS hot spots (i.e. the area on vessel surface with SWS above a given threshold, namely the median value of SWS at baseline angiogram).

Table 1
Definition of superficial wall strain parameters.

Measurements	Units	Definitions/specifications
Peak-SWS	Dimensionless	Maximum value of SWS within cardiac cycle over the specific vessel segment (e.g. proximal or distal edge, treated segment)
SA-SWS	Dimensionless	Derived from the mean SWS at the local finite elements over the specific segments
TA-SWS	Dimensionless	Derived from the summation of SWS during cardiac cycle divided by time period
Surface area of high SWS	mm^2	The area of the finite element on vessel surface with SWS value that is higher than the median value of SWS on the entire artery at baseline

SA: segment averaged; SWS: superficial wall strain; TA: time averaged.

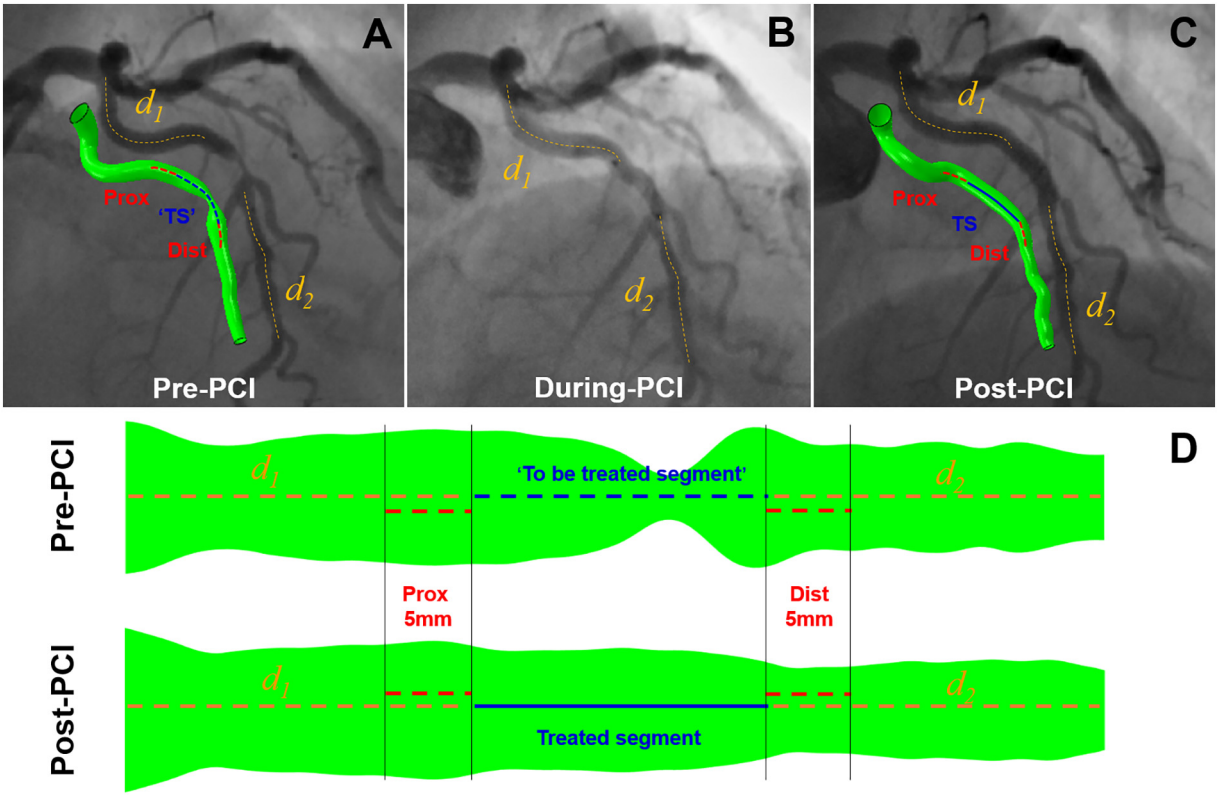

Fig. 1. Segments of interest matching pre- and post-procedure
According to the proximal and distal distances, the "to be treated" segments (A) were identified on the pre-procedure angiograms and 3D models.
During procedure, visible contour of balloon inflation with two radio-opaque markers were used to measure the distance between the proximal (d1) and distal (d2) markers with respect to major bifurcations (B).
Post-PCI, the "treated" segments (C) were identified on the post-procedure angiograms and 3D models. The implanted vessel segment (TS) and 5 mm proximal and distal edges were identified with the 3D centerline from the device edges (A pre-procedure and C post-procedure).
(D) The spread-out view of the three segments of interest matching pre- and post-PCI.

2.5. Definitions of interested segments

To assess the variations in QCA and SWS, the vessel segments of interest were defined as "to be treated" or treated segment immediately after PCI or at 5-year follow-up, plus 5 mm proximal and 5 mm distal to the device edges (Fig. 1). First, the two radio-opaque markers on the BRS or the deflated balloon of the DES at both ends on post-PCI angiogram were used to define the scaffolded/stented segment on the 3D

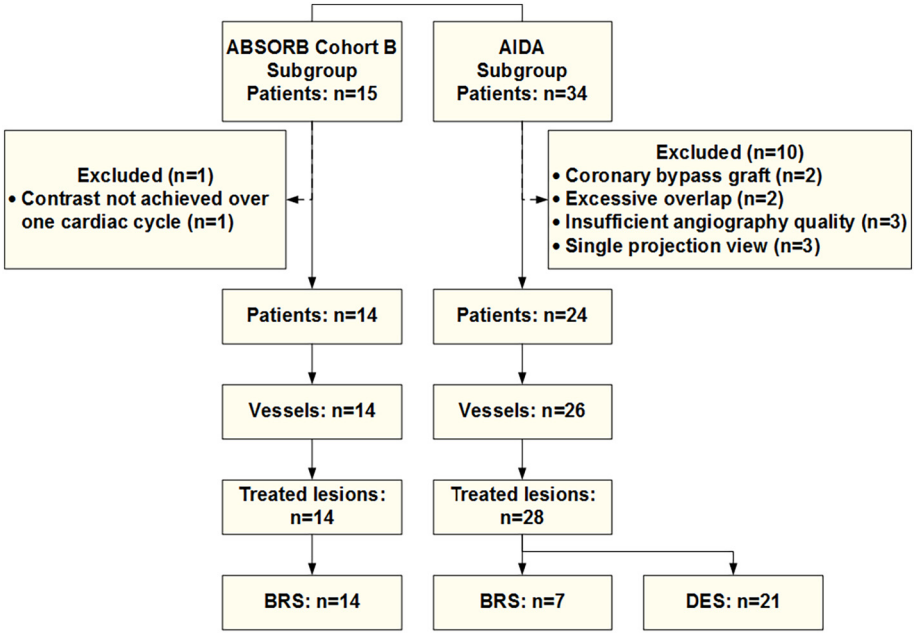

Fig. 2. Schematic representation of patients, vessels, and treated lesions included in this study.

Table 2
Baseline patient characteristics.

	Total (38 Pts, 42 TLs)	BRS (21 Pts, 21 TLs)	DES (17 Pts, 21 TLs)	P
Age (years)	63.2 ± 11.7	62.7 ± 8.83	63.8 ± 14.9	0.788
Male	26 (68.4)	12 (57.1)	14 (82.4)	0.161
Cardiovascular risk factors				
Hypertension requiring medication	23 (60.5)	14 (66.9)	9 (52.9)	0.509
Diabetes mellitus requiring medication	9 (23.7)	5 (23.8)	4 (23.5)	1.000
Hypercholesterolemia requiring medication	18 (47.4)	13 (61.9)	5 (29.4)	0.058
Current smokers	11 (28.9)	8 (38.1)	3 (17.6)	0.282
Myocardial infarction history	8 (21.1)	4 (19.0)	4 (23.5)	1.000
Clinical presentation				
Non-ST-elevation myocardial infarction	4 (10.5)	0 (0.0)	4 (23.5)	0.032
ST-elevation myocardial infarction	7 (18.4)	3 (14.3)	4 (23.5)	0.678
Unstable angina	6 (15.8)	4 (19.0)	2 (11.8)	0.672
Chronic coronary syndrome	20 (52.6)	13 (61.9)	7 (41.2)	0.328
Target vessel				
Left anterior descending coronary artery	20 (52.6)	10 (47.6)	10 (58.8)	0.532
Left circumflex coronary artery	11 (28.9)	5 (23.8)	6 (35.3)	0.491
Right coronary artery	9 (23.7)	6 (28.6)	3 (17.6)	0.476

BRS: bioresorbable scaffold; DES: drug-eluting stent; Pts: Patients; TLs: Treated lesions.
Note: In the DES group, RCA in 1 patient treated with 2 DESs, and LCx in other 1 patient treated with 2 DESs.
Values are % (count/sample size) or mean ± SD.

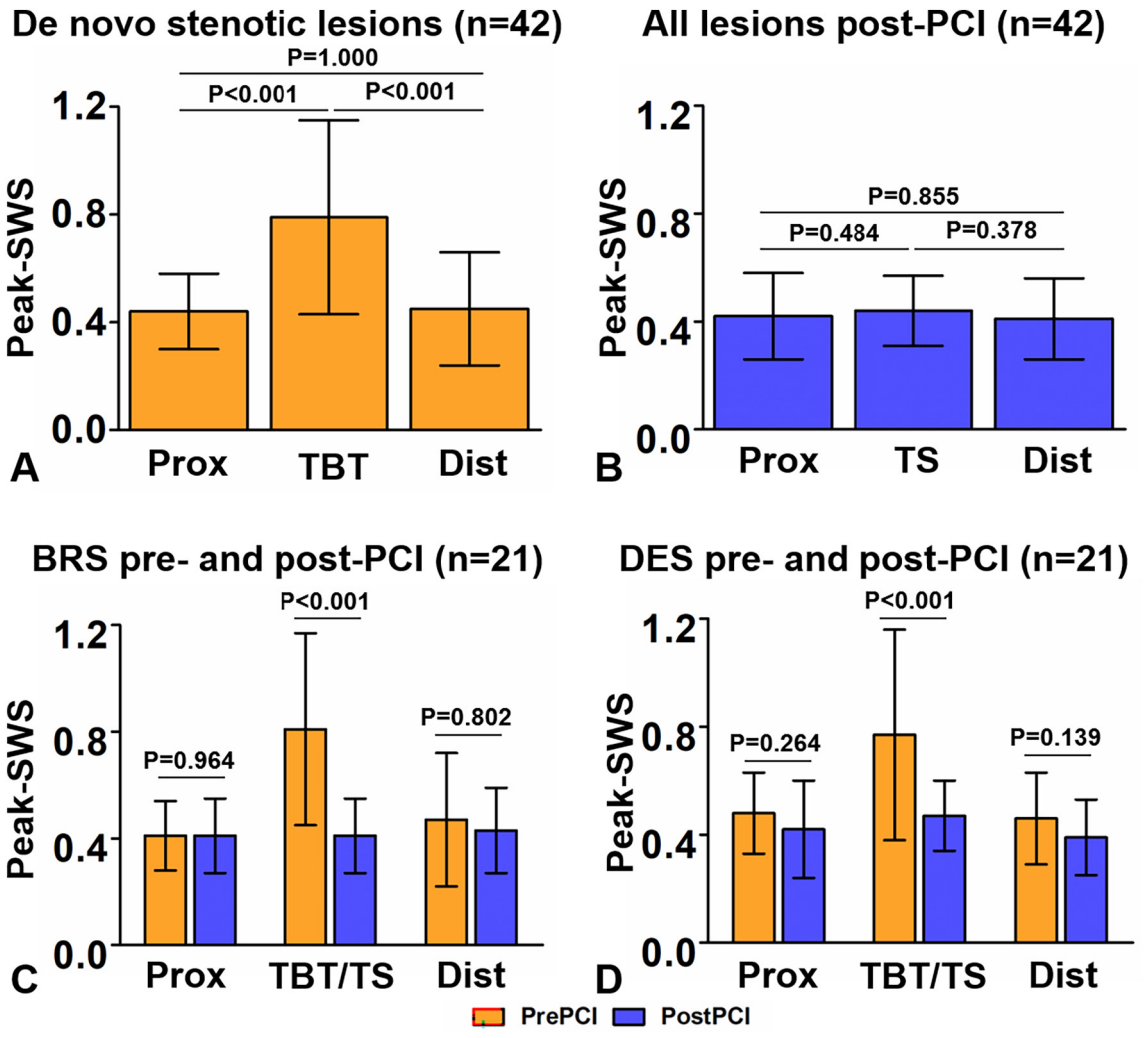

Fig. 3. Peak superficial wall strain in the three segments pre- and post-PCI
(A) The peak SWS in the "to be treated" segment is significantly higher than that in the proximal and distal edges for all de novo stenotic lesions. (B) At post-PCI, the peak SWS was reduced to levels similar to those measured at proximal and distal edges. The peak SWS changes pre- and post-PCI in the (C) BRS and (D) DES group.
Dist: distal edge; Prox: proximal edge; SWS: superficial wall strain; TBT: "to be treated" segment; TS: treated segment.

reconstructed vessel centerlines. Then, the major side branches next to the device segment were identified, and the distances along the centerline from both side branches to the end of the device segment were measured. Finally, the distance between side branches on the centerline was used for longitudinal matching of the segments of interest on serial angiograms. The proximal and distal edges were further identified as 5-mm long segments adjacent to the device. The morphological and mechanical variables were calculated for each segment.

2.6. Statistical analysis

Categorical variables are presented as counts and percentages and tested with Fisher's exact-test. Continuous data were presented as means ± standard deviations or median with 25th and 75th percentiles as appropriate. Normality distribution of the data was determined with the Shapiro-Wilk test. For overall assessment, differences in the variables of the QCA and SWS among the three interested segments ("to be treated" or treated segment, 5-mm segments at the proximal and distal edges) were evaluated by Student *t*-test or Mann–Whitney *U* test, as appropriate. A Kruskal–Wallis H test was used for comparing three segment groups. Statistical significance was further examined by post-hoc testing to determine paired differences of three segment groups, using Bonferroni correction to account for multiple tests. The surface area of SWS hot spots was calculated based on a threshold defined by the median value of the SWS distribution on the analyzed vessel at pre-PCI. Changes in the SWS between baseline and post-PCI were evaluated by means of Student *t*-test or paired Wilcoxon singed rank test. Comparison between BRS and DES groups was analyzed by Student *t*-test and Chi square test, or Fisher's exact test when Cochran's rule was not met. Absolute changes (differences) for each variable were calculated as post-PCI minus pre-PCI values. Relative changes (percent difference) for each variable were calculated as (post-PCI minus pre-PCI values)/ pre-PCI values × 100. All statistical tests were two-sided and a $p < 0.05$ was considered statistically significant, except the Bonferroni-adjusted *p* values. All analyses were performed with IBM SPSS (v22.0, SPSS Inc., Chicago, Illinois).

3. Results

3.1. Studied population and baseline characteristics

A total of 49 patients were selected from the ABSORB Cohort B trial ($n = 15$) and AIDA trial ($n = 34$). Ten patients were excluded due to pre-defined criteria (Fig. 2). A subgroup of 14 patients from

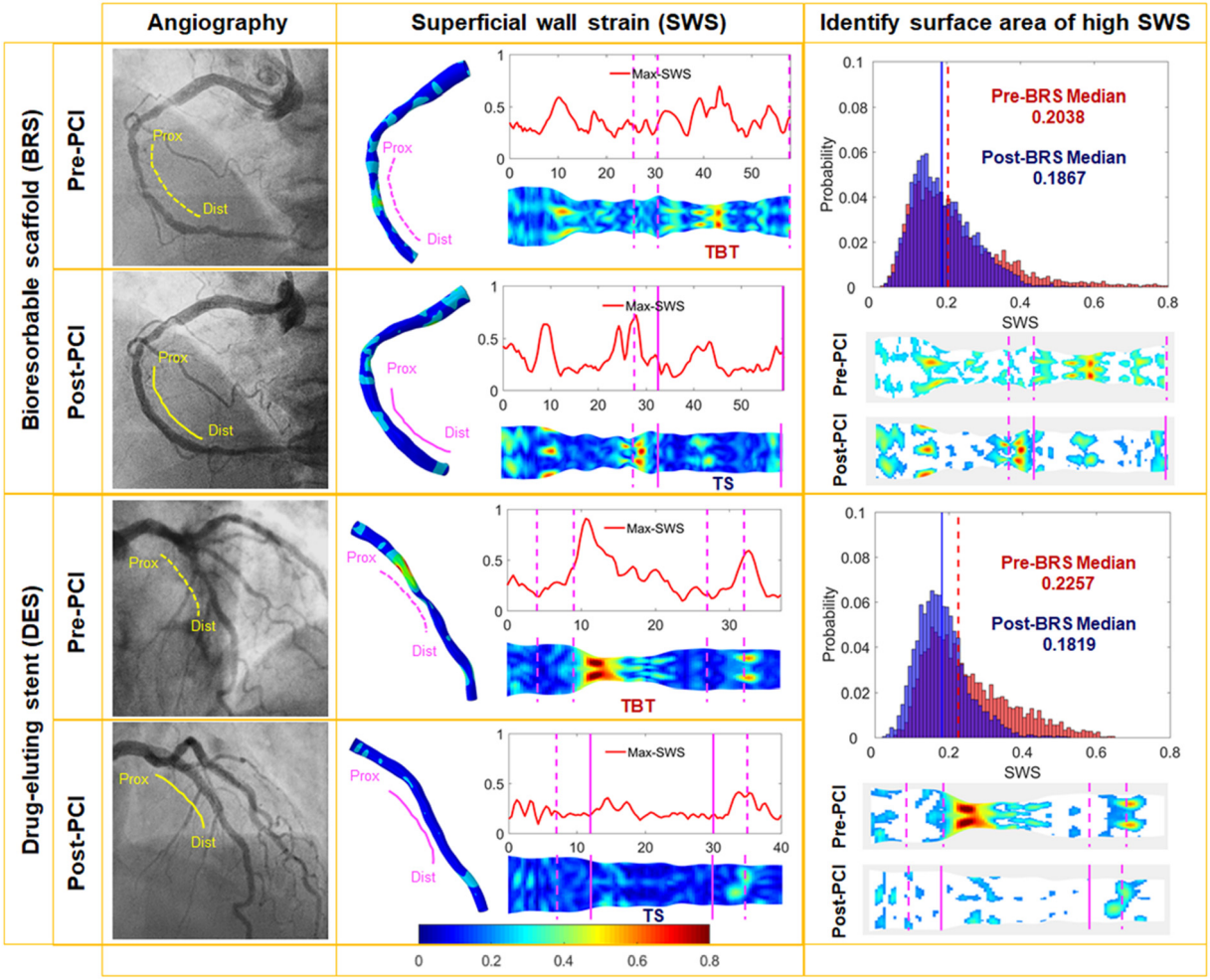

Fig. 4. Illustrative examples of SWS at pre- and post-PCI treated with BRS or DES
After the implantation of scaffold/stent, the SWS on the treated segments were significantly reduced, while SWS relocation occurs on the device edges. Angiography pre- and post-PCI is shown on the left.
Superficial wall strain (SWS) in 3D, spread-out view (2D) and longitudinal curve (1D) shown in the middle.
On the right, the surface area of high-SWS was identified by the finite element of vessel wall with the SWS value higher than the median value of SWS at pre-PCI. BRS data are shown on the top two panels and DES on the bottom two panels, at pre- and post-PCI for each device.

ABSORB trial was selected to investigate SWS after complete absorption of the scaffold. Baseline characteristics of the patients are shown in Table 2. There was a greater prevalence of patients with non-ST-elevation myocardial infarction in DES versus BRS group (23.5 % vs. 0.0 %, $p = 0.032$). Ninety-four analyses of SWS were performed on the forty vessels (20 left anterior descending arteries; 11 left circumflex coronary arteries, 9 right coronary arteries) during baseline, post-PCI and follow-up.

3.2. Baseline SWS of stenotic coronary arteries

Before PCI, the peak SWS on the "to be treated" segments (0.79 ± 0.36) was significantly higher than at the proximal (0.44 ± 0.14, $p < 0.001$) and distal (0.45 ± 0.21, $p < 0.001$) edges (Fig. 3). The surface area of the high-SWS on the "to be treated" segments (66.62 ± 25.96 mm^2) was significantly higher than at the proximal (18.93 ± 12.55 mm^2, $p < 0.001$) and distal (15.15 ± 13.25 mm^2, $p < 0.001$) edges. The segment-averaged SWS on the "to be treated" segments (0.41 ± 0.13) was not different from proximal edges (0.35 ± 0.13, $p = 0.124$), but significantly higher than at distal edges (0.33 ± 0.15, $p < 0.05$).

3.3. Acute changes in SWS after PCI treated by BRS or DES

3.3.1. Variation of QCA after PCI

From pre- to post-PCI, QCA parameters at the "to be treated" segments were not different between BRS and DES groups (Supplemental Table 1). MLD increased significantly from 0.99 ± 0.39 mm to 2.11 ± 0.40 mm in BRS group (1.12 [0.87,1.36] mm, $p < 0.001$) and from 1.09 ± 0.45 mm to 2.24 ± 0.52 mm in DES group (1.15 [0.85,1.46] mm, $p < 0.001$). Before treatment, BRS group showed a smaller MLD and MLA, but larger AS% at proximal edges compared with DES (all $p < 0.05$). After treatment, no significant difference of these four QCA parameters was observed between two groups.

3.4. Immediate effect of PCI on SWS at the treated segment

After device implantation, the peak SWS on the treated segments of all cases was significantly decreased by 0.44 ± 0.13 and became similar to the values at the proximal and distal edges (0.42 ± 0.16, $p = 0.484$; and 0.41 ± 0.15, $p = 0.378$, respectively) (Fig. 3). The surface area of high SWS was significantly reduced by 42.42 ± 31.18 mm^2. Representative examples of computation of angiography-based SWS at pre- and post-PCI after BRS or DES treatment are shown in Fig. 4. All the SWS

Table 3
Immediate effect of PCI on SWS of coronary arteries treated with BRS or DES.

SWS	Devices	Pre-PCI	Post-PCI	Absolute difference (95 % CI)	Relative changes (%) (95 % CI)	P
Proximal edges (21 paired measurements)						
Peak-SWS	BRS	0.41 ± 0.13	0.41 ± 0.14	−0.00(−0.09,0.08)	−2.63(−26.10,20.98)	0.964
	DES	0.48 ± 0.15	0.42 ± 0.18	−0.06(−0.16,0.04)	−15.52(−40.13,23.95)	0.264
	P	0.101	0.749	0.297	0.345	
Surface area-hSWS (mm^2)	BRS	17.73 ± 13.14	18.54 ± 13.95	0.81(−7.64,9.26)	4.00(−21.60,38.84)	0.847
	DES	20.13 ± 12.14	17.59 ± 29.28	−2.54(−16.52,11.64)	−27.08(−89.60,10.76)	0.716
	P	0.542	0.894	0.568	0.212	
SA-SWS	BRS	0.34 ± 0.13	0.30 ± 0.09	−0.03(−0.1,0.04)	−5.56(−20.14,14.58)	0.381
	DES	0.36 ± 0.13	0.29 ± 0.11	−0.07(−0.14,0.00)	−18.75(−45.56,13.45)	0.055
	P	0.515	0.644	0.338	0.551	
TA-SWS	BRS	0.19 ± 0.10	0.18 ± 0.09	−0.02(−0.06,0.03)	−7.14(−26.60,13.25)	0.462
	DES	0.21 ± 0.07	0.19 ± 0.07	−0.02(−0.07,0.02)	−20.00(−41.43,28.64)	0.272
	P	0.656	0.906	0.739	0.936	
Before/after treated segment (21 paired measurements)						
Peak-SWS	BRS	0.81 ± 0.36	0.41 ± 0.14	−0.39(−0.55,-0.23)	−46.91(−61.58,-30.23)	0.000
	DES	0.77 ± 0.39	0.47 ± 0.13	−0.31(−0.49,-0.13)	−41.38(−55.27,-2.71)	0.001
	P	0.775	0.183	0.432	0.255	
Surface area-hSWS (mm^2)	BRS	64.14 ± 18.34	45.20 ± 32.31	−18.94(−35.33,-2.56)	−28.03(−67.41,5.59)	0.025
	DES	69.10 ± 32.13	39.65 ± 30.55	−29.45(−49.01,-9.90)	−50.90(−76.30,6.52)	0.004
	P	0.543	0.570	0.398	0.889	
SA-SWS	BRS	0.43 ± 0.15	0.26 ± 0.09	−0.16(−0.24,-0.09)	−36.73(−55.97,-11.71)	0.000
	DES	0.39 ± 0.12	0.27 ± 0.08	−0.12(−0.19,-0.06)	−36.11(−49.42,-18.07)	0.000
	P	0.442	0.840	0.406	0.397	
TA-SWS	BRS	0.24 ± 0.02	0.16 ± 0.01	−0.08(−0.13,-0.04)	−39.13(−48.81,-18.63)	0.001
	DES	0.23 ± 0.07	0.17 ± 0.05	−0.06(−0.10,-0.02)	−26.32(−47.05,-5.31)	0.002
	P	0.559	0.603	0.363	0.242	
Distal edges (21 paired measurements)						
Peak-SWS	BRS	0.47 ± 0.25	0.43 ± 0.16	−0.02(−0.15,0.12)	3.03(−23.91,32.92)	0.802
	DES	0.46 ± 0.17	0.39 ± 0.14	−0.07(−0.17,0.02)	−18.18(−34.89,26.24)	0.139
	P	0.837	0.382	0.362	0.286	
Surface area-hSWS (mm^2)	BRS	13.36 ± 10.15	17.84 ± 11.43	4.48(−2.26,11.22)	13.92(−23.26,102.66)	0.187
	DES	16.94 ± 15.81	16.29 ± 29.85	−0.65(−15.55,14.25)	−24.26(−73.09,61.80)	0.930
	P	0.387	0.826	0.422	0.245	
SA-SWS	BRS	0.33 ± 0.18	0.32 ± 0.13	−0.01(−0.11,0.08)	0.00(−21.48,51.49)	0.776
	DES	0.33 ± 0.13	0.29 ± 0.10	−0.05(−0.12,0.02)	−5.26(−38.77,27.59)	0.176
	P	0.913	0.424	0.487	0.420	
TA-SWS	BRS	0.19 ± 0.02	0.18 ± 0.02	−0.01(−0.07,0.05)	4.00(−28.28,57.29)	0.820
	DES	0.20 ± 0.09	0.19 ± 0.07	−0.02(−0.06,0.03)	0.00(−26.71,42.28)	0.534
	P	0.647	0.847	0.782	0.702	

Values are mean ± SD.
BRS: bioresorbable scaffold; DES: drug-eluting stent; PCI: percutaneous coronary intervention; SWS: superficial wall strain; SA: segment-averaged; TA: time-averaged.
[a] Absolute difference = Post-PCI - Pre-PCI. Relative changes (%) = Difference /Pre-PCI*100.

parameters on the treated segments are significantly decreased at post-PCI ($p < 0.05$), regardless of BRS or DES implant (Table 3). However, the mean value of the surface area of high-SWS was decreased by 29.45 (9.90,49.01) mm^2 in DES group versus 18.94 (2.56,35.33) mm^2 in BRS group ($p < 0.05$), respectively.

3.5. Relocation of high SWS at device edges after PCI

Although no statistically significant absolute or relative difference in SWS variables was found at both edges, individual responses were variable (Fig. 5). High SWS values were often shifted to proximal edges in 18 of 42 cases (42.9 %) and to distal edges in 17 of 42 cases (40.5 %). An increase of peak SWS after PCI at the proximal edge was observed in 10 of 21 cases (48.6 %) in BRS group, in 8 of 21 cases (38.1 %) in DES group, respectively. For peak SWS, an increase at the distal edge was found in 11 (52.4 %) cases in the BRS group and 6 (28.6 %) cases in DES group (Fig. 5).

3.6. Correlation between SWS and QCA

The correlations between SWS and QCA variables at each segment of interest are summarized in Supplemental Table 2. There is a negative correlation between four SWS variables and MLD as well as MLA, while positive correlations are observed between SWS variables and DS% as well as AS%. Of those, the best correlation was found between peak SWS and AS% ($\rho = 0.405$, $p < 0.001$). Scatterplots are presented in Supplemental Figs. 1–4.

3.7. Long-term variations of SWS in BRS subgroup

3.7.1. QCA at long-term follow-up

The results of serial assessment of QCA parameters at baseline, post-PCI and long-term follow-up in BRS subgroup are presented in Supplemental Table 3. At 5-year follow-up, the QCA parameters of the treated segments had similar values compared with those at post-PCI and remained significantly different from pre-PCI ($p < 0.001$). No significant differences at both edges were found neither at baseline, post-PCI or at follow-up.

3.8. Serial assessment of SWS in the BRS subgroup

A representative case of SWS at pre-, post-PCI and follow-up treated by BRS is shown in Fig. 6. At 5-year follow-up, there were significant differences in the SWS parameters (except for surface area of high SWS) at the treated segments when compared with those at pre-PCI, while no significant differences at both edges were found among pre-, post-PCI and follow-up (Table 4). At follow-up, the surface area of high SWS in the treated segments (46.13 ± 37.46 mm^2) was similar to post-PCI (45.73 ± 37.06 mm^2, $p = 0.978$) and tended to be lower than at pre-PCI (61.47 ± 14.06 mm^2, $p = 0.163$).

3.9. Correlation between SWS and QCA in the BRS subgroup

We observed a negative nonlinear correlation between MLD and peak SWS (peak SWS $= -0.16 \times \text{MLD}^3 + 1.1 \times \text{MLD}^2 - 2.4 \times \text{MLD} + 2.2$)

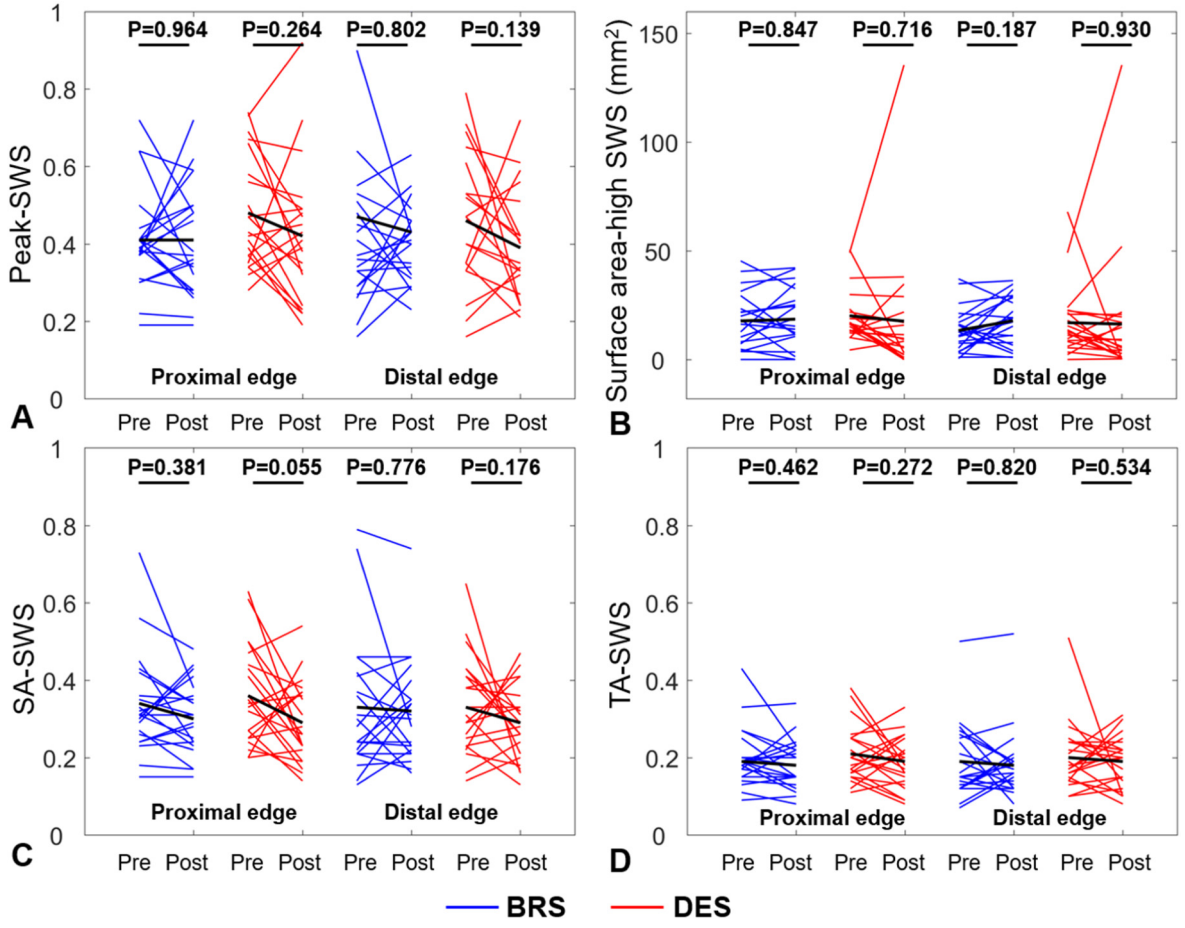

Fig. 5. Individual SWS changes in both edges at pre- and post-PCI
(A) peak-SWS; (B) surface area-high SWS; (C) segment-averaged SWS; (D) time-averaged SWS.
BRS (Blue) and DES (Red).

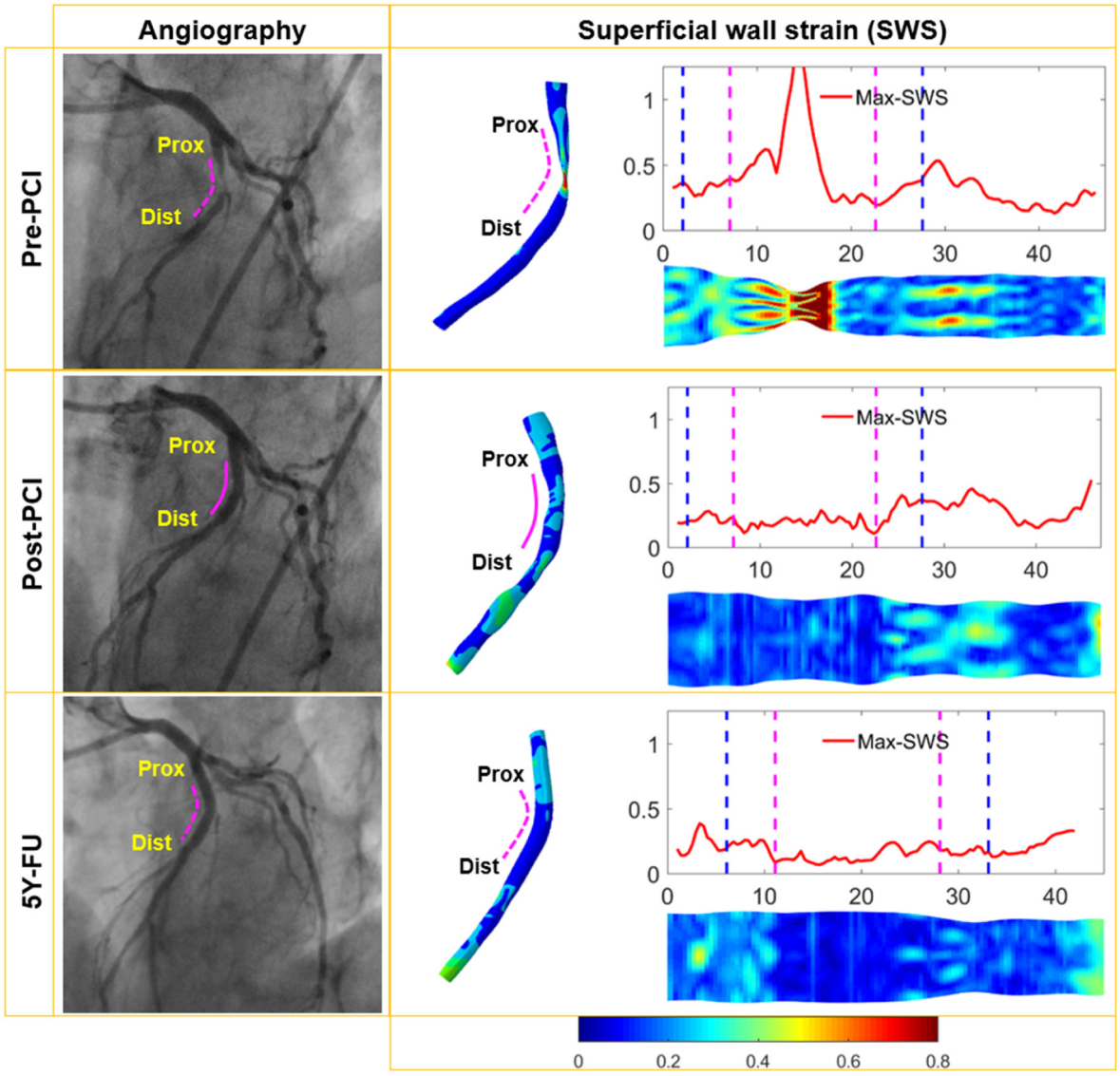

Fig. 6. An illustrative example of the serial SWS of vessel treated with BRS
Compared to values pre-PCI, there was strong evidence for a reduction in peak-SWS on the treated segments immediately after PCI and at 5-year follow-up. (Left) Angiography at pre-, post-PCI and 5-year follow-up; (right) SWS in 3D, spread-out view (2D) and longitudinal curve (1D).

(Fig. 7). The MLD before PCI at treated segment (1.04 ± 0.42 mm) was significantly increased after PCI (2.16 ± 0.35 mm, $p < 0.001$) and remained unchanged at follow-up (1.98 ± 0.31 mm, $p < 0.001$) (Supplemental Table 3). While the peak SWS before PCI at treated segment (0.79 ± 0.37) was significantly decreased after PCI (0.36 ± 0.09, $p < 0.001$) and remained low at follow-up (0.40 ± 0.12, $p = 0.001$) (Table 4).

4. Discussion

The main findings of the present study can be summarized as follows: 1) The angiography-based SWS provided a comprehensive assessment of morphological and mechanical status of coronary artery at baseline, post-PCI and follow-up. 2) At pre-PCI, the SWS in lesion segments of de novo stenotic arteries is significantly higher than in normal segments. 3) Following device implant, the SWS in the treated segments was significantly decreased. The immediate effect of PCI by BRS or DES shows a similar decrease of SWS, suggesting that, after proper vessel pre-dilatation, BRS provides comparable scaffolding to DES. Relocation of high SWS to device edges was observed in both groups after PCI. 4) At long-term follow-up, the SWS in BRS subgroup remains low and without evidence of any change at both edges across pre-, post-PCI and 5-year follow-up.

The QCA results from pre- to post-PCI showed the expected acute gain in the lesion segments (Supplemental Table 1). When compared with BRS, the increase of MLD in distal edge is significantly larger after DES than that in proximal edge ($p < 0.001$). This observation is in agreement with previous reports showing modified vessel geometry at the distal edge [15,16], perhaps due to high pressure balloon post-dilatation. The peak SWS has the best correlation with AS% ($\rho = 0.405$, $p < 0.001$). As shown in Supplemental Table 1, AS% at proximal edges is significant different between BRS and DES, unlike DS%.

Before procedure, the peak SWS on “to be treated” segment was significantly higher than proximal and distal edges ($p < 0.001$). This might be explained by heterogeneous plaque composition and complex lumen geometry, in contrast with the more homogeneous normal vessel segments. It should be noted that the peak SWS levels at the normal segments at pre- and post-PCI are very similar, and also similar to the value at the treated segment after device implantation.

Table 4
Changes in the SWS parameters at the three segments at pre-, post-PCI and follow-up of BRS (Absorb trial).

SWS	Difference (95 % CI)								
	Pre-PCI	Post-PCI	5y-FU	Post-Pre	P	5yFU-Post	P	5yFU-Pre	P
Proximal edges (14 vessels)									
Peak-SWS	0.39 ± 0.11	0.38 ± 0.13	0.34 ± 0.12	−0.01 (−0.10,0.09)	0.914	−0.05 (−0.15,0.05)	0.332	−0.05 (−0.14,0.04)	0.242
SA-hSWS (mm^2)	18.77 ± 12.73	18.68 ± 14.25	16.69 ± 13.34	−0.09 (−10.59,10.41)	0.986	−1.99 (−12.71,8.73)	0.706	−2.08 (−12.21,8.05)	0.676
SA-SWS	0.29 ± 0.08	0.28 ± 0.09	0.26 ± 0.09	−0.01 (−0.08,0.05)	0.653	−0.02 (−0.09,0.05)	0.544	−0.04 (−0.10,0.03)	0.282
TA-SWS	0.17 ± 0.04	0.16 ± 0.05	0.15 ± 0.06	−0.01 (−0.05,0.03)	0.586	−0.01 (−0.05,0.03)	0.593	−0.02 (−0.06,0.02)	0.266
Before and after treated segment (14 vessels)									
Peak-SWS	0.79 ± 0.37	0.36 ± 0.09	0.40 ± 0.12	−0.43 (−0.64,-0.22)	0.000	0.04 (−0.04,0.13)	0.319	−0.39 (−0.61,-0.17)	0.001
SA-hSWS (mm^2)	61.47 ± 14.06	45.73 ± 37.06	46.13 ± 37.46	−15.74 (−37.52,6.04)	0.149	0.40 (−28.55,29.35)	0.978	−15.34 (−37.32,6.64)	0.163
SA-SWS	0.41 ± 0.16	0.23 ± 0.06	0.25 ± 0.09	−0.18 (−0.27,-0.09)	0.000	0.02 (−0.04,0.13)	0.472	−0.16 (−0.26,-0.06)	0.002
TA-SWS	0.23 ± 0.08	0.13 ± 0.03	0.15 ± 0.06	−0.09 (−0.14,-0.05)	0.000	0.02 (−0.02,0.05)	0.381	−0.08 (−0.13,-0.02)	0.009
Distal edges (14 vessels)									
Peak-SWS	0.40 ± 0.18	0.40 ± 0.11	0.45 ± 0.24	0.00 (−0.12,0.12)	0.980	0.05 (−0.10,0.19)	0.528	0.05 (−0.12,0.21)	0.564
SA-hSWS (mm^2)	15.16 ± 10.89	18.92 ± 11.22	16.27 ± 12.93	3.76 (−4.83,12.35)	0.377	−2.64 (−12.05,6.76)	0.569	1.12 (−8.17,10.41)	0.807
SA-SWS	0.31 ± 0.16	0.28 ± 0.10	0.32 ± 0.13	−0.03 (−0.14,0.07)	0.497	0.42 (−0.05,0.13)	0.344	0.01 (−0.10,0.12)	0.877
TA-SWS	0.17 ± 0.07	0.16 ± 0.05	0.20 ± 0.12	−0.01 (−0.06,0.03)	0.556	0.04 (−0.03,0.11)	0.295	0.02 (−0.05,0.10)	0.522

MLD: minimum lumen diameter; DS%: percent diameter stenosis; SA-hSWS: surface area of high SWS.

The notable reduction of SWS immediately after implanting either BRS or DES can be attributed to the scaffolding effect of the device. This finding is in agreement with the previously reported decrease in strain after Absorb BVS 1.1 implant measured by palpography on intravascular ultrasound [17]. Wall strain measured by palpography is based on the difference in the longitudinal intravascular ultrasound cross-sections between pre- and post-PCI and the estimated results are likely influenced by the location of the cross-section and artifactual acoustic properties of stent struts [18,19]. In our study, angiography-based SWS is measured from the deformation of coronary vessel during the entire cardiac cycle.

The clinical utility of biodegradable scaffolds is currently challenged based on worse mid-term clinical outcomes than durable metallic DES [20]. At the same time, it is essential to verify in vivo that BRS have sufficient radial surface force to maintain luminal expansion shortly after implant as well as after bioabsorption of the polymeric device. The general concept is that the stent/scaffold should exert enough radial support to prevent elastic recoil and be flexible enough to adapt to the tortuosity of the vessel. In the present study, we found no difference in QCA and SWS variables at pre- and post-PCI between BRS and DES implants (Table 3), in spite of huge differences in tensile stress. This can be explained by the effect of pre-dilatation causing plaque fractures and dissections that allow proper device expansion and maintained scaffolding. It is also possible that the increased strut thickness and width of BRS compensates for reduced radial support compared to cobalt-chromium alloy [14]. On average, device implantation did not significantly affect SWS at the proximal and distal edges before and after PCI, neither with BRS or DES (Table 3). These results are similar to previous reports [9,17]. Of note, there are 29 to 62 % of cases with elevated SWS at either device edge, which may be associated with later stenosis [17,18,21].

After implant, the deployed device changes the morphology of the lumen-plaque interface with a significant decrease in SWS. At 5-year

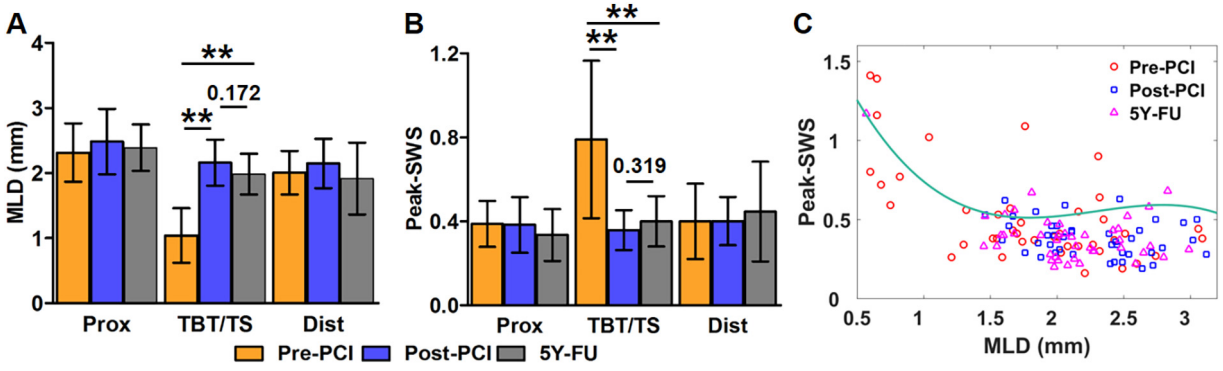

Fig. 7. MLD and peak SWS in BRS subgroup at pre-, post-PCI and follow-up
(A) MLD at the "before/after implanted" segment was significantly increased after PCI and remained at 5Y-FU; (B) SWS at the "before/after implanted" segment was significantly decreased after PCI and remain at 5Y-FU; (C) Nonlinear negative correlation between MLD and SWS was found (peak SWS = $-0.16 \times MLD^3 + 1.1 \times MLD^2 - 2.4 \times MLD + 2.2$).

follow-up, the SWS remained at post-PCI levels, suggesting that the previously scaffolded lumen-vessel interface might become less vulnerable to plaque events or stenosis progression. These observations expand the previously reported OCT study showing that the dilated lumen was preserved even after the complete degradation of scaffolds with compressed plaque within the wall [22].

4.1. Study limitations

Although this is the first comprehensive study of angiography-based SWS in de novo arteries at pre-, post-PCI and follow-up, some limitations should be acknowledged. Firstly, matching of the segments across three timepoints using marker locations could be affected by variations of arterial lengths during cardiac cycle, leading to inaccurate delineation of proximal or distal edges. Secondly, the 3D arterial reconstruction based on angiography at two projections might be inaccurate in asymmetrical stenosis. Of note, the same angiographic projections at pre- and post-PCI, even at follow-up in the ABSORB Cohort B subgroup were used for 3D reconstruction in order to reduce variability in SWS computation. Finally, the precise wall strain near the deployed strut (0.1 mm width) was smoothed and likely underestimated due to the current resolution of angiographic images.

5. Conclusions

The quantitative assessment of SWS from angiography has the potential to provide valuable information about the mechanical status of coronary arteries in vivo. The SWS was high at stenotic coronary segments and was significantly reduced by PCI to a similar extent by metallic stents and polymer-based scaffolds. On average, device implantation did not significantly affect proximal and distal stent edges. The long-term follow-up 5 years after BRS implant shows maintained low SWS of the treated coronary segment, after complete biosorption of the polymer.

Declaration of competing interest

Y. Onuma reports institutional research grants related to his work as the chairman of cardiovascular imaging core labs of several clinical trials and registry sponsored by industry, for which they receive no direct compensation. P. W. Serruys reports personal fees from Sino Medical Sciences Technology, Philips/Volcano, Xeltis, outside the submitted work. S. Tu reports grants and consultancy from Pulse Medical. Authors have no other disclosures or financial involvement with any organization or entity with a financial interest in or financial conflict with the subject matter or materials discussed in the manuscript apart from those disclosed.

Appendix A. Supplementary data

Supplementary data to this article can be found online at https://doi.org/10.1016/j.carrev.2023.03.005.

References

[1] Schaar JA, Regar E, Mastik F, et al. Incidence of high-strain patterns in human coronary arteries: assessment with three-dimensional intravascular palpography and correlation with clinical presentation. Circulation. 2004;109:2716–9.
[2] Wu X, von Birgelen C, Muramatsu T, et al. A novel four-dimensional angiographic approach to assess dynamic superficial wall stress of coronary arteries in vivo: initial experience in evaluating vessel sites with subsequent plaque rupture. EuroIntervention. 2017;13:1099–103.
[3] Costopoulos C, Maehara A, Huang Y, et al. Heterogeneity of plaque structural stress is increased in plaques leading to MACE: insights from the PROSPECT study. J Am Coll Cardiol Img. 2020;13:1206–18.
[4] Wu X, von Birgelen C, Wijns W, et al. Superficial wall stress assessed from 4-D analysis of coronary angiography in vivo. Int J Cardiovasc Imaging. 2017;33:1–2.
[5] Wu X, von Birgelen C, Li Z, et al. Assessment of superficial coronary vessel wall deformation and stress: validation of in silico models and human coronary arteries in vivo. Int J Cardiovasc Imaging. 2018;34:1–13.
[6] Wu X, Ono M, Kawashima H, et al. Angiography-based 4-dimensional superficial wall strain and stress: a new diagnostic tool in the catheterization laboratory. Front Cardiovasc Med. 2021;8:667310.
[7] Serruys PW, Ormiston JA, Onuma Y, et al. A bioabsorbable everolimus-eluting coronary stent system (ABSORB): 2-year outcomes and results from multiple imaging methods. Lancent. 2009;373:897–910.
[8] Brugaletta S, Gogas BD, Garcia-Garcia HM, et al. Vascular compliance changes of the coronary vessel wall after bioresorbable vascular scaffold implantation in the treated and adjacent segments. Circ J. 2012;76:1616–23.
[9] Van Mieghem CA, McFadden EP, de Feyter PJ, et al. Noninvasive detection of subclinical coronary atherosclerosis coupled with assessment of changes in plaque characteristics using novel invasive imaging modalities: the Integrated Biomarker and Imaging Study (IBIS). J Am Coll Cardiol. 2006;47:1134–42.
[10] Wu X, Lunardi M, Elkoumy A, et al. A novel angiography-based computational modelling for assessing the dynamic stress and quantitative fatigue fracture risk of the coronary stents immediately after implantation: effects of stent materials, designs and target vessel motions. Med Nov Technol Devices. 2022:14.
[11] Kereiakes DJ, Onuma Y, Serruys PW, et al. Bioresorbable vascular scaffolds for coronary revascularization. Circulation. 2016;134:168–82.
[12] Serruys PW, Onuma Y, Dudek D, et al. Evaluation of the second generation of a bioresorbable everolimus-eluting vascular scaffold for the treatment of de novo coronary artery stenosis. J Am Coll Cardiol. 2011;58:1578–88.
[13] Wykrzykowska JJ, Kraak RP, Hofma SH, et al. Bioresorbable scaffolds versus metallic stents in routine PCI. N Engl J Med. 2017;376:2319–28.
[14] Wu X, Wu S, Kawashima H, et al. Current perspectives on bioresorbable scaffolds in coronary intervention and other fields. Expert Rev Med Devices. 2021;18:351–66.
[15] Gogas BD, Bourantas CV, Garcia-Garcia HM, et al. The edge vascular response following implantation of the absorb everolimus-eluting bioresorbable vascular scaffold and the XIENCE V metallic everolimus-eluting stent. First serial follow-up assessment at six months and two years: insights from the first-in-man ABSORB cohort B and SPIRIT II trials. EuroIntervention. 2013;9:709–20.
[16] Kim JW, Suh SY, Choi CU, et al. Six-month comparison of coronary endothelial dysfunction associated with sirolimus-eluting stent versus paclitaxel-eluting stent. J Am Coll Cardiol Intv. 2008;1:65–71.
[17] Bourantas CV, Garcia-Garcia HM, Campos CAM, et al. Implications of a bioresorbable vascular scaffold implantation on vessel wall strain of the treated and the adjacent segments. Int J Cardiovasc Imaging. 2014;30:477–84.
[18] Schaar JA, van der Steen AFW, Mastik F, et al. Intravascular palpography for vulnerable plaque assessment. J Am Coll Cardiol. 2006;47:C86–91.
[19] Bruining N, Winter Sd, Roelandt JRTC, et al. Monitoring in vivo absorption of a drug-eluting bioabsorbable stent with intravascular ultrasound-derived parameters. J Am Coll Cardiol Intv. 2010;3:449–56.
[20] Garcia-Garcia HM, Serruys PW, Campos CM, et al. Assessing bioresorbable coronary devices: methods and parameters. J Am Coll Cardiol Img. 2014;7:1130–48.
[21] Tateishi H, Suwannasom P, Sotomi Y, et al. Edge vascular response after resorption of the everolimus-eluting bioresorbable vascular scaffold: a 5-year serial optical coherence tomography study. Circ J. 2016;80:1131–41.
[22] Zeng YP, Tateishi H, Cavalcante R, et al. Serial assessment of tissue precursors and progression of coronary calcification analyzed by fusion of IVUS and OCT 5-year follow-up of scaffolded and nonscaffolded arteries. J Am Coll Cardiol Img. 2017;10:1151–61.